JOURNAL OF MATERIALS SCIENCE 32 (1997) 4793–4802

The structure of the calcium silicate hydrate phases present in hardened pastes of white Portland cement/blast-furnace slag blends

I. G. RICHARDSON
Materials Unit, Department of Civil Engineering, University of Leeds, Leeds LS2 9JT, UK
G. W. GROVES
Department of Materials, University of Oxford, Parks Road, Oxford OX1 3PH, UK

The C-S-H gels present in both water- and alkali-activated hardened pastes of white Portland cement/blast-furnace slag blends have been studied by solid-state ^{29}Si magic angle spinning nuclear magnetic resonance (NMR) spectroscopy and analytical transmission electron microscopy (TEM). Structural data are obtained by NMR for the semi-crystalline C-S-H gels in the alkali-activated systems and extended to the nearly amorphous gels in the water-activated systems by peak broadening; unambiguous chemical analyses are determined in the TEM. The following conclusions apply to both the semi-crystalline and nearly amorphous C-S-H gels: (1) aluminium substitutes for silicon at tetrahedral sites; (2) aluminium only substitutes for silicon in the central tetrahedron of pentameric silicate chains; (3) the results strengthen confidence in dreierkette-based models for the structure of C-S-H. Compositional similarities suggest that these conclusions will be true for OPC/slag blends, and possibly also for OPC/pulverized fuel ash blends indicating that the same structural model applies to C-S-H gels in a wide range of hardened cement pastes.

1. Introduction

The cementing medium in modern Portland cement-based concretes can include several inorganic by-product materials, including ground granulated blast-furnace slag (ggbs)*, pulverized fuel ash (pfa)†, and microsilica.†† Whatever its exact composition, the main hydration products and principal binding phases in all calcium silicate-based pastes and concrete are calcium silicate hydrate (C-S-H) gels. Understanding the nature of C-S-H is therefore important.

In any given system there are generally two morphologically distinct types of C-S-H: inner product (Ip), formed within the boundaries of the original anhydrous grains, and outer product (Op), formed in the originally water or solution-filled spaces. Ip regions most commonly have a compact, fine-scale and homogeneous morphology whereas Op C-S-H exhibits a strongly linear, directional morphology as seen by transmission electron microscopy (TEM). In blast-furnace slag/Portland cement blends, this fibrillar character is gradually replaced as the fraction of slag is increased by a C-S-H with a foil-like morphology [1].

The composition and the degree of structural order of C-S-H phases depends on the nature of the system: for example, in water-activated Portland cement-based systems the C-S-H is nearly amorphous whereas more crystalline phases can be formed by hydrothermal reaction or by the reaction of cement with concentrated alkali hydroxide solutions. In most systems of commercial interest C-S-H gels are at best poorly crystalline, and generally nearly amorphous. Although this has made studying the structure of C-S-H phases difficult, the weight of experimental evidence indicates a structural relationship with the crystalline mineral 1.4-nm tobermorite and possibly with jennite. Studies by trimethylsilylation (TMS) [2] and solid-state nuclear magnetic resonance spectroscopy (NMR) [3, 4] have established that C-S-H in young pastes consists mainly of dimeric silicate chains. The TMS studies have indicated that in older pastes some of the dimers are linked by monomers to form pentamers [5, 6], and then possibly the dimers and pentamers are linked by monomers to form octamers [5]; thus suggesting a 2, 5, 8, … $(3n - 1)$ chain length sequence, where $n = 1, 2, 3$, etc. This led Taylor [7] to propose a model based on finite silicate units derived from the "dreierkette" structures of 1.4-nm tobermorite and jennite by the omission of some or all of the bridging tetrahedra. Fig. 1a shows a schematic

*a by-product of the manufacture of pig-iron
†a by-product from coal-fired power stations
††a by-product from the silicon industry

0022–2461

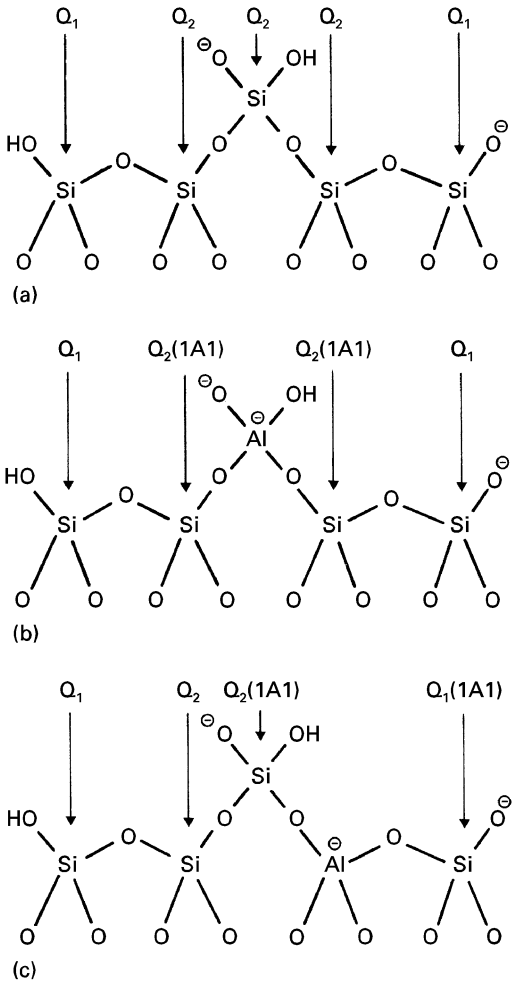

Figure 1 (a) Schematic representation of a pentameric silicate chain of the type present in Taylor's model [7]. Q_1 and Q_2 units are identified; the middle Q_2 unit is the "bridging" tetrahedron. (b) Same as (a), but with Al^{3+} substituted for Si^{4+} in the bridging tetrahedron. (c) Same as (a), but with Al^{3+} substituted for Si^{4+} in a non-bridging Q_2 tetrahedron.

representation of a pentameric silicate chain of the type present in Taylor's model. The O atoms at the bottom of the figure are also part of the central CaO_2 layer.

In ordinary portland cement (OPC) and blended cements, C-S-H accommodates substituent ions, the most important of which is aluminium [1, 8]. The only technique capable of giving unambiguous compositions for C-S-H gels present in hardened cement pastes is X-ray microanalysis of thinned sections in the TEM. Using this technique, Richardson and Groves [1, 8] showed that over a range of ggbs/OPC blends there was a linear relationship between an increase in the R/Ca ratio (where R is a trivalent cation, mainly Al^{3+}) and an increase in the Si/Ca ratio. Taylor [9, 10] considered that the higher Al contents could be accounted for by considering the analysed volume to be a very intimate mixture of C-S-H with a low Al content with layers of AFm structure (AFm (Al_2O_3-Fe_2O_3-mono) phases have the general formula $[Ca_2(Al\,Fe)(OH)_6]\cdot X\cdot xH_2O$ where X denotes one formula unit of a singly charged anion, a half a formula unit of a doubly charged anion) and have layer structures derived from that of calcium hydroxide by the ordered replacement of one Ca^{2+} ion in three by Ae^{3+} or Fe^{2+}.). This would appear unlikely because it would mean that the lower Ca/Si ratio system would have to have more AFm – a Ca-rich phase – than the higher Ca/Si ratio systems. It is also unlikely that such a mixture would occur on such a fine scale ($\ll 300$ nm) so as to produce a smooth compositional trend from the small regions analysed in the TEM. There is now direct experimental evidence against this postulate; electron energy loss spectroscopy (EELS) studies of C-S-H in KOH activated blast furnace slags [11, 12] and 9/1 slag/OPC [13] have shown that the Al is in predominantly 4-fold co-ordination: admixture with an AFm phase would have shown in addition Al present in 6-fold co-ordination.

Richardson and Groves took the compositional relationship to support a structural limitation on the level of Al substitution where Al substitutes for Si at tetrahedral sites. This led them to propose a general model for the structure of substituted C-S-H gels [14, 15], in which the mean silicate chain length increases as the Si/Ca ratio increases, with Al substituting for Si in bridging tetrahedra of a dreierkette chain structure. The model may be represented as:

$$\{Ca_{2n}H_w(Si_{1-a}R^{[4]}_a)_{(3n-1)}O_{(9n-2)}\}$$
$$I^{c+}_{a/c\,(3n-1)}(OH)_{w+n(y-2)}Ca_{n\cdot y/2}\cdot mH_2O \qquad (1)$$

where,

$$0 \leqslant y \leqslant 2; \quad n(2-y) \leqslant w \leqslant 2n$$
$$2 \leqslant y \leqslant 4; \quad 0 \leqslant w \leqslant 2n$$
$$4 \leqslant y \leqslant 6; \quad 0 \leqslant w \leqslant n(6-y)$$

The model – which is based on a tobermorite-like core (that of the formula contained within the braces) – consists of a highly disordered layer structure comprising finite silicate chains of length $3n-1$. For individual structural units $n = 1, 2, 3, \ldots$ etc. but it has effective non-integer values for mixtures of units of different length. In immature cement pastes dimer is the most abundant silicate species ($n = 1$). These are linked during polymerization by bridging tetrahedra to form pentamer ($n = 2$) and higher polymers; in formula 1 there are $n-1$ bridging sites. $R^{[4]}$ is a trivalent cation, mainly Al^{3+}, in tetrahedral co-ordination and I^{c+} is an interlayer ion, either a monovalent alkali cation or Ca^{2+}, charge-balancing the R^{3+} substitution for Si^{4+}. Aluminium is assumed to only substitute for Si in the bridging tetrahedra of the dreierketten structure, thus, $0 \leqslant a \leqslant n - 1/3n - 1$.

The model can be interpreted in terms of either of the two most common approaches to the structure of C-S-H, namely a mixture of structural units based on the minerals jennite and 1.4 nm-tobermorite [7] or tobermorite-based units in "solid-solution" with $Ca(OH)_2$ [16–20]. From the tobermorite/$Ca(OH)_2$ viewpoint it is better to represent the model by formula 2,

$$Ca_xH_{(6n-2x)}(Si_{1-a}R^{[4]}_a)_{(3n-1)}O_{(9n-2)}I^{c+}_{a/c\,(3n-1)}$$
$$z\,Ca(OH)_2\cdot mH_2O \qquad (2)$$

where,

$$x = \tfrac{1}{2}(6n - w); \quad z = \tfrac{1}{2}(w + n(y - 2))$$

Note that when $n = 1$ (i.e., a dimer) formula 2 reduces to that used by Glasser *et al.* [21] to describe the C-S-H predominant in young OPC pastes.

Taylor's model distinguishes clearly between main layer and interlayer Ca^{2+} ions but his assertion [9] that no distinction is made in Richardson and Groves' formulations is not true. For example, in formula 14 of reference [14],

$$\{Ca_{2n}H_wSi_{(3n-1)}O_{(9n-2)}\}\,(OH)_{w+n(y-2)}$$
$$Ca_{n\cdot y/2}\cdot mH_2O \qquad (3)$$

the $2n$ Ca^{2+} ions within the braces are always main layer Ca^{2+} ions, while there are always $n - w/2$ interlayer Ca^{2+} ions required for charge balance. The position of the remainder of the $n\cdot y/2$ Ca^{2+} ions outside the braces depends on the structural viewpoint adopted. From the tobermorite/$Ca(OH)_2$ viewpoint they occur in layers of $Ca(OH)_2$ sandwiched between silicate layers of tobermorite-like structure while from the jennite/tobermorite viewpoint they form part of the main layer (as ≡ Si–O–Ca–OH). The parameters in the formula may of course vary from one region to another of the gel accounting for the local variations in composition observed by TEM.

In Taylor's model there is one silanol group per three tetrahedral sites [7], which is given by $w = n$ in formula 1, and this is probably the most reasonable assumption for Portland cement-based systems cured at normal temperatures – a point supported later in this paper. However, the compositions and mean chain lengths of some C-S-H gels put them outside this assumption [22] so the extra flexibility in the possible degree of protonation inherent in formula 1 is necessary.

Significant progress has been made towards establishing satisfactory experimental verification for the substituted general model; it successfully links the chemical composition and silicate anion structure of low Ca/Si ratio C-S-H phases [14]; and it is supported by the work of Brydson *et al.* [11] and Richardson *et al.* [11, 22] on the determination of the location of Al in semi-crystalline substituted C-S-H gels. The latter were formed by the reaction of a ggbs [11, 12] and synthetic slag glass [12, 22] with 5M KOH solution. The single-pulse ^{29}Si and ^{1}H–^{29}Si cross-polarization (CP) magic-angle spinning (MAS) NMR spectra for these gels gave conclusive evidence for the Al substituting for Si solely in the central tetrahedron of pentameric linear chains, as illustrated in Fig. 1b. This followed from the absence of a peak corresponding to $Q_1(1A1)$[§] units on the ^{29}Si CP MAS NMR spectra; such units would be expected if – assuming no chain terminating Al–Al substituted for Si at tetrahedral sites other than in the bridging tetrahedra, as in Fig. 1c. There could be no significant numbers of chain terminating Al as this would have produced higher Al/Si ratios calculated by NMR than derived from analytical TEM which gives unambiguous compositions for the C-S-H gels; in fact, there was good agreement.

However, is this model for the structure of substituted C-S-H gels valid for those present in water-activated pastes at compositions relevant to concrete? Such phases are nearly amorphous which makes them less-easily studied by NMR; a decrease in long-range structural order leads to broader NMR peaks and reduced resolution. We have approached this problem by comparing the nature of the C-S-H gels formed in slag/white Portland cement (WPC) blends when activated by water and by 5M KOH solution: structural data is obtained by NMR for the semi-crystalline C-S-H gels in the KOH-activated systems and extended to the water-activated systems by peak broadening; unambiguous chemical analyses are determined in the TEM. The results are presented in this paper.

2. Experimental procedures

The commercial slag was supplied by AEA Technology Harwell Laboratory. The oxide composition is given in Table 1. Powder X-ray diffraction (XRD) revealed no crystalline phases. The cement used was a white Portland cement from the Aalborg company (Bogue composition (wt %): 65% C_3S, 22% C_2S, 4% C_3A, 1% C_4AF). A white Portland cement was used because of its low Fe content; the presence of paramagnetic ions causes peak broadening in NMR.

Pastes of 9/1 and 1/1 ggbs/WPC were mixed with a water: solids ratio or solution:solids ratio of 0.4 and placed in sealed plastic tubes for curing in a water bath at 25 °C. Freshly ground samples were used for X-ray diffraction and NMR. For TEM, the reaction was stopped by outgassing under vacuum. Sections of the hardened pastes were prepared for TEM by argon ion-beam milling as reported elsewhere [24]. After they had been coated with carbon, specimens were examined in a Jeol 2000FX TEM equipped with a Tracor Northern TN5500 X-ray microanalysis system. The microscope was operated at 200 kV. Calibration factors were established using åkermanite ($Ca_2MgSi_2O_7$), wollastonite ($CaSiO_3$), $Ca_3Al_2O_6$, $CaSO_4$, K_2SO_4 and FeS.

Specimens for NMR spectroscopy were ground to a powder and packed into zirconia rotors. The single-pulse ^{29}Si and ^{1}H–^{29}Si cross polarization (CP) spectra were acquired using a Bruker MSL-200 spectrometer (magnetic field 4.7 T; operating frequencies of 200.13 MHz for ^{1}H and 39.76 MHz for ^{29}Si). The spectra were acquired with MAS at ≈ 3 kHz in 7 mm

[§]In silicates, solid state ^{29}Si MAS NMR can provide quantitative information on the fractions of silicon present in different tetrahedral environments, Q_n ($0 \leqslant n \leqslant 4$), where Q is a silicate tetrahedron and n denotes the number of oxygens which bridge to adjacent tetrahedra. Increased polymerization of the Q_n building units causes characteristic up-field chemical shifts. In aluminosilicates the shifts are further influenced by the replacement of Si by Al in tetrahedra adjacent to a given Si site, generally producing down-field shifts of ≈ 3 → 5 ppm per Al [23]. There are thus 15 possible Q_n (mAl) structural units where Q is a silicate tetrahedron connected via oxygen bridges to m Al and n-m other Si atoms, with $n = 0$ to 4 and $m = 0$ to n [23].

TABLE I Oxide composition of the ggbs determined by wavelength dispersive X-ray analysis (mean $\pm \sigma_{n-1}$; 73 analyses)

Oxide	wt%	Oxide	wt%
Na_2O	0.27 ± 0.07	K_2O	0.65 ± 0.14
MgO	7.83 ± 0.26	CaO	40.73 ± 0.90
Al_2O_3	12.27 ± 0.46	TiO_2	0.64 ± 0.08
SiO_2	36.13 ± 0.68	MnO	0.65 ± 0.17
S^{2-}	0.83 ± 0.12	FeO	low

rotors, and with high-power proton decoupling at a field of approximately 60 kHz. The single pulse spectra were acquired over 32 000 → 42 000 scans using a pulse recycle delay of 2 s and a flip angle of 45°. Approximate spin-lattice relaxation time (T_1) measurements indicated that saturation effects were not significant for the hydrate peaks. The CP spectra were acquired over ≈ 30 000 scans with a contact time of 1 ms and a recycle delay time of 2 s. For CP, the Hartmann–Hahn condition was set using kaolinite [25]. The ^{29}Si chemical shifts are given relative to tetramethylsilane (TMS) at 0 ppm, with kaolinite used as an external standard at −91.2 ppm. For all spectra, 2048 points were acquired at a sweep width of 15 151 Hz, apodized with 10 Hz of exponential line broadening, and zero filled to 8192 point prior to Fourier transformation. The spectra were iteratively fitted to Voigt line shapes using the software Igor [26] with additional macros written by Brough [27]. The full procedure is outlined in the Results section.

Samples for thermal analysis were crushed, washed in propan-2-ol, filtered, and stored in a vacuum desiccator. A Mettler DSC 20 differential scanning calorimeter was used over a temperature range of 50–600 °C at a heating rate of 10 °C min^{-1} and in an atmosphere of air.

3. Results and discussion

3.1. Hydration products and microstructure

The $Ca(OH)_2$ present in slag/OPC blends is generally observed as large plates, most commonly in the Op region [1, 8]. This was the case in the water-activated pastes studied here, but in the KOH-activated pastes it occurred as microcrystals intimately mixed on a nanometer scale with layers of C-S-H; this is illustrated in Fig. 2, a TEM micrograph of a typical region in the KOH-activated neat WPC paste. This admixture of phases is most clearly evident in the central and lower right of the micrograph; inset is a selected area electron diffraction pattern of the central region showing reflections characteristic of microcrystalline $Ca(OH)_2$. The presence of microcrystalline $Ca(OH)_2$ is consistent with the broader peaks observed in the powder XRD traces of the KOH-activated pastes than in those with water. Regarding the models for the structure of C-S-H, the presence of finely admixed C-S-H and $Ca(OH)_2$ is consistent with – but not proof of – treating the C-S-H as a low Ca/Si ratio C-S-H–$Ca(OH)_2$ "solid-solution."

The microstructures of the water activated ggbs/WPC blends were very similar to ggbs/OPC

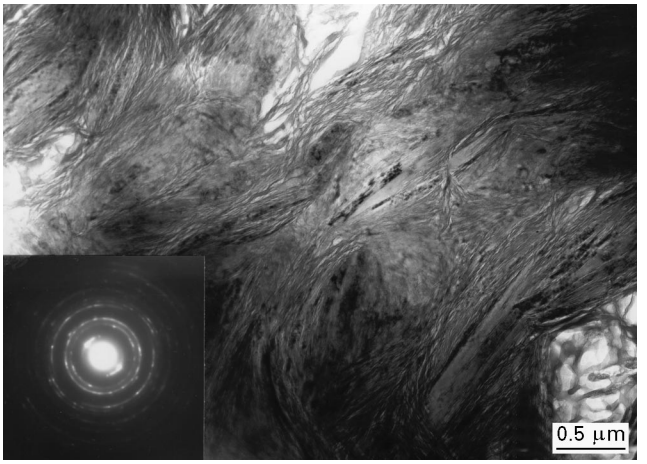

Figure 2 A typical region of Op in a KOH-activated neat WPC paste. Inset is a selected area electron diffraction pattern from the central region showing reflections characteristic of microcrystalline $Ca(OH)_2$. The mean Ca/Si ratio of 12 regions giving similar patterns was 6.7 ± 2.3 indicating that the regions consist of $Ca(OH)_2$ microcrystals admixed with C-S-H at the nanometre level.

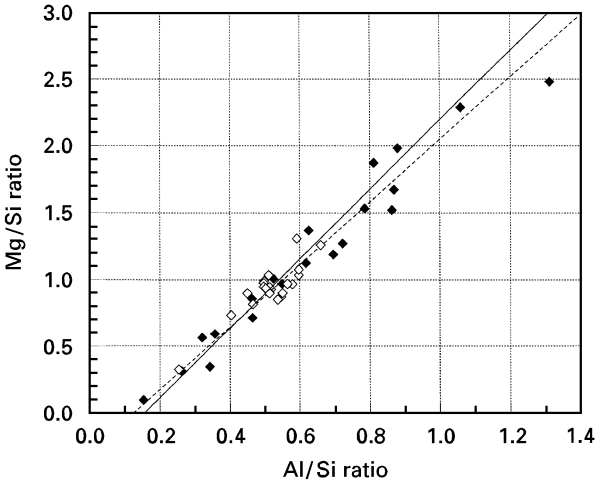

Figure 3 Mg/Si against Al/Si ratio plot for analyses of slag Ip present in the slag/WPC 9/1 pastes. (◆) 9:1/water; (– – –) Al/Si = 0.1257 + (0.4268 × Mg/Si) $R^2 = 0.95$; (◇) 9:1/KOH and (—) Al/Si = 0.1562 + (0.3843 × Mg/Si) $R^2 = 0.78$.

pastes: the microstructures are similar to those described in reference [1]. As in those pastes the C-S-H, which is nearly amorphous, is present in two morphologically distinct forms: Ip and Op. The C-S-H in the KOH systems is also present as Ip and Op but it is semi-crystalline, giving electron diffraction patterns similar to the example in reference [22] for C-S-H in a neat ggbs/KOH paste. Ip could again be considered an intimate mixture of C-S-H and a Mg, Al hydroxide type phase. This is illustrated on Fig. 3 for the 9/1 pastes: for example, the Al/Mg ratio of the Mg, Al hydroxide phase in the water-activated paste is 0.43.

3.2. Chemical composition of the C-S-H gels

Fig. 4 incorporates some earlier data of Richardson and Groves' [1, 15] for a range of ggbs/OPC blends hydrated at 20 °C for 14 months (water/cement (W/C) = 0.4) (●), some ggbs/KOH pastes made with the same slag (■), and a synthetic slag/KOH paste (▲)

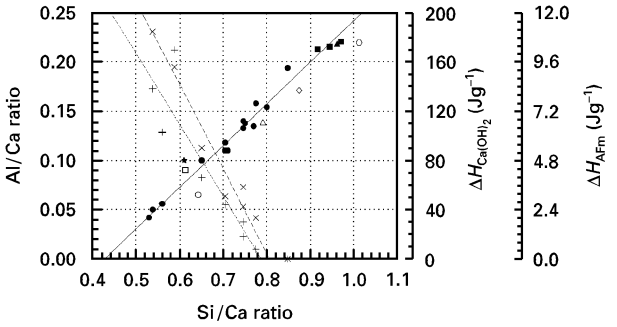

Figure 4 Al/Ca against Si/Ca ratio plot of TEM analyses of Op C-S-H present in various slag containing systems. Each point corresponds to a mean value of 20 to 50 analyses which are unambiguously of Op C-S-H. The filled and open symbols correspond to systems with different slags and with ordinary and white Portland cements respectively. The regression line is for the filled symbols only. The figure also includes plots of AFm (×) and $Ca(OH)_2$ (+) against Si/Ca ratio of the Op C-S-H present in the slag/OPC blends. Note that although there is no AFm or $Ca(OH)_2$ present in neat slag/water systems AFm is present when slag is activated by KOH solutions; these data are not shown. Point ★ corresponds to the approximate composition of the C-S-H in an OPC/28% wt pfa blend [28]. (●) OPC/slag blends [1, 15]; (■) 100% slag/5M KOH; (▲) synthetic slag/5M KOH [22]; (○) 50% WPC 50% slag/water; (□) 50% WPC 50% slag/5M KOH; (△) 10% WPC 90% slag/water; (◇) 10% WPC 90% slag/5M KOH; (◌) 100% slag/5M KOH. The lines represent: (—) Si/Ca = 0.4277 + (2.366 × Al/Ca) $R^2 = 0.98$; (----) Si/Ca = 0.7873 − (0.0017 × $\triangle H_{CaOH_2}$) $R^2 = 0.83$ and (– –) Si/Ca = 0.8065 − (0.0243 × $\triangle H_{AFM}$) $R^2 = 0.95$.

[22]. Fig. 4 shows that the decrease in Ca/Si ratio and increase in Al/Ca ratio is accompanied by a reduction in the levels of $Ca(OH)_2$ and AFm as determined by differential scanning calorimetry.

The maximum Ca/Si ratio possible for C-S-H in these systems (indicated by the point at which the regression line meets the *x*-axis) would appear to be ≈ 2.3, and the maximum Ca/Si ratio possible for C-S-H with no $Ca(OH)_2$ or AFm present is ≈ 1.25. Interestingly, these compositions correspond to the maximum compositions in Taylor's model for jennite- and tobermorite-based structural units (J_{dimer} Ca/Si = 2.25; T_{dimer}Ca/Si = 1.25). This would appear to agree with his contention that there are generally *n* silanol groups per structural unit, i.e., $w = n$ in formula 1. Structural units with all their bridging tetrahedra occupied by Al^{3+} would also have a Ca/Si ratio of 1.25 if the extra charge were balanced by either alkali cations or H^+.

Although the Op C-S-H was often admixed with $Ca(OH)_2$ on a very fine scale as in Fig. 2, it was also present alone in areas sufficiently large to enable chemical analysis, for example in Fig. 5 (centre and lower right). The compositions of the Op C-S-H gels present in both the KOH- and water-activated ggbs/WPC pastes are included on Fig. 4 (open symbols) for comparison with the ggbs/OPC blends and slag/KOH. It can be seen that they fall on the same compositional trend line, despite having different Portland cements and different blast-furnace slags. This suggests that the results of this study are probably relevant for Portland cement-containing systems in general. It is also likely that they are also relevant to pfa/OPC blends; point ★ on Fig. 4 corresponds to the

Figure 5 TEM micrograph of an Op region in the KOH-activated neat WPC paste. Op C-S-H not admixed with $Ca(OH)_2$ is present in the centre and lower right of the micrograph.

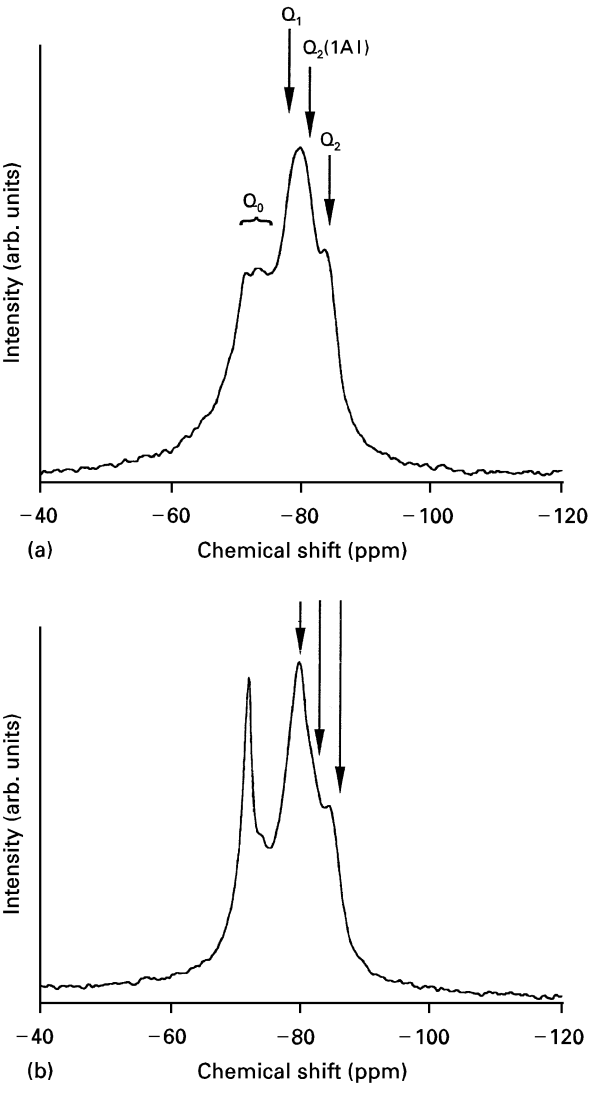

Figure 6 Single pulse ^{29}Si MAS NMR spectra for the water-activated (a) 9/1 and (b) 1/1 slag/WPC blends hydrated for 3 weeks. Approximate chemical shifts for the expected hydrate peaks are shown i.e., Q_1, Q_2(1Al), and Q_2(0Al).

approximate composition of the C-S-H in an OPC 28 wt % pfa blend [28]. The proximity of this point to the compositional trend line suggests that there may be a universal compositional relationship for the

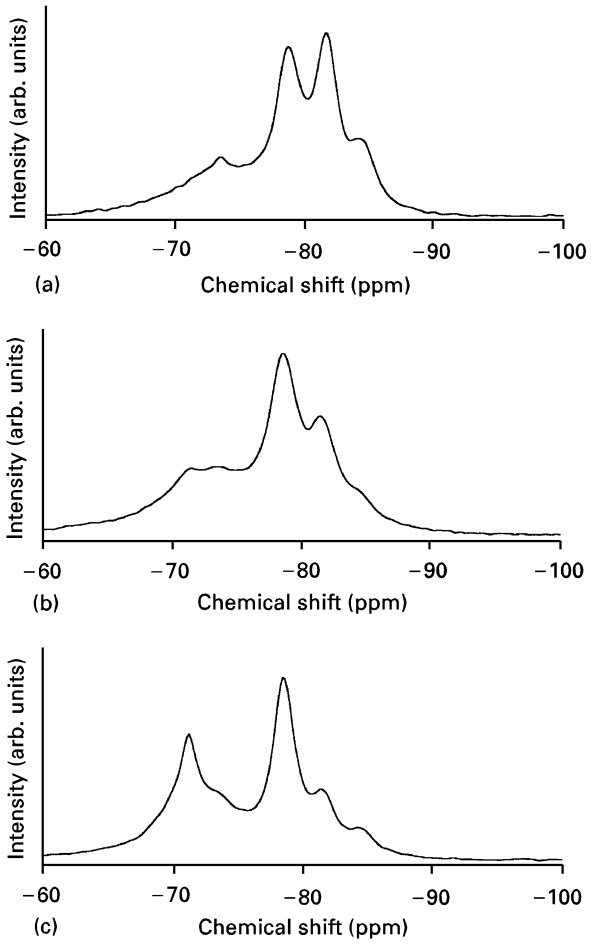

Figure 7 Single pulse ^{29}Si MAS NMR spectra for the 5M KOH-activated (a) neat slag, (b) 9/1, and (c) 1/1 slag/WPC blends hydrated for one, three, and four days respectively. The hydrate peaks are well-defined with approximate chemical shifts of -78.7 ppm (Q_1), -81.7 ppm (Q_2(1Al)), and -84.5 ppm (Q_2(0Al)).

C-S-H phases present in all cementitious calcium alumino-silicate systems.

3.3. NMR results

Fig. 6(a and b) shows the single-pulse ^{29}Si NMR spectra for water-activated 9/1 and 1/1 ggbs/WPC blends. The Q_0 peaks correspond to unreacted slag and belite (the sharp component); it is assumed that all the alite has reacted. Both the spectra appear to have three hydrate peaks, Q_1, Q_2(1Al), and Q_2, but they are not well-resolved; it would not be possible to deconvolute these spectra without more information.

Fig. 7(a–c) shows the corresponding spectra for the KOH-activated blends, and also for the neat slag/KOH paste; the hydrate peaks are very clearly defined. These spectra were deconvoluted and the results used to aid deconvolution of the water-activated spectra in Fig. 6(a and b).

3.3.1 Procedure for the deconvolution of the NMR spectra

The spectra were iteratively fitted to Voigt line shapes using the software Igor [26] with additional macros written by Brough [27]. The fitting function used can handle four peaks (centre bands), each with first order spinning side bands. The 28 fitting coefficients are summarized in Table II.

The stages in the deconvolution procedure were as follows:

3.3.1.1 Stage 1. A baseline was fitted to the spectrum using the regions between the peaks and sidebands.

3.3.1.2 Stage 2. Since the spectra have five centre bands and the program can only handle four it was necessary to model one of the peaks and subtract a contribution from it from each of the spectra. The belite peak was selected because it is sharp and well-defined and a good model could be easily obtained from a spectrum of a hydrated KOH-activated WPC whose alite had reacted completely. This peak was then superimposed on the KOH-activated spectra and the intensity and linewidth altered so as to give a residual peak shape centred on ≈ -73 ppm that was characteristic of the unreacted slag: the alite in the blends was assumed to have reached a high degree of reaction. This assumption is considered reasonable since the alite in the neat WPC of the same age had largely reacted and the presence of slag would be expected to enhance the degree of early alite reaction [29].

3.3.1.3 Stage 3. The spectra resulting from stage 2 had four distinct centre bands. The centre bands were then iteratively fitted to Voigt lineshapes (a convolution of Lorentzian and Gaussian). It was found necessary to constrain the linewidths of the smaller hydrate peaks (Q_2(0Al) and Q_2(1Al)) to be the same as the largest (Q_1).

TABLE II Designation of the coefficients used in the fitting function [27]
K0 → K3 Baseline (4th order polynomial)
K4 Spinning speed

1st peak slag	2nd peak Q_1	3rd peak Q_2(1Al)	4th peak Q_2(0Al)	
K5	K11	K17	K23	Intensity – left side band
K6	K12	K18	K24	Intensity – centre band
K7	K13	K19	K25	Intensity – right side band
K8	K14	K20	K26	Peak position in ppm
K9	K15	K21[a]	K27[a]	Linewidth
K10	K16	K22[b]	K28[b]	Lineshape

[a]Same as K15
[b]Same as K16

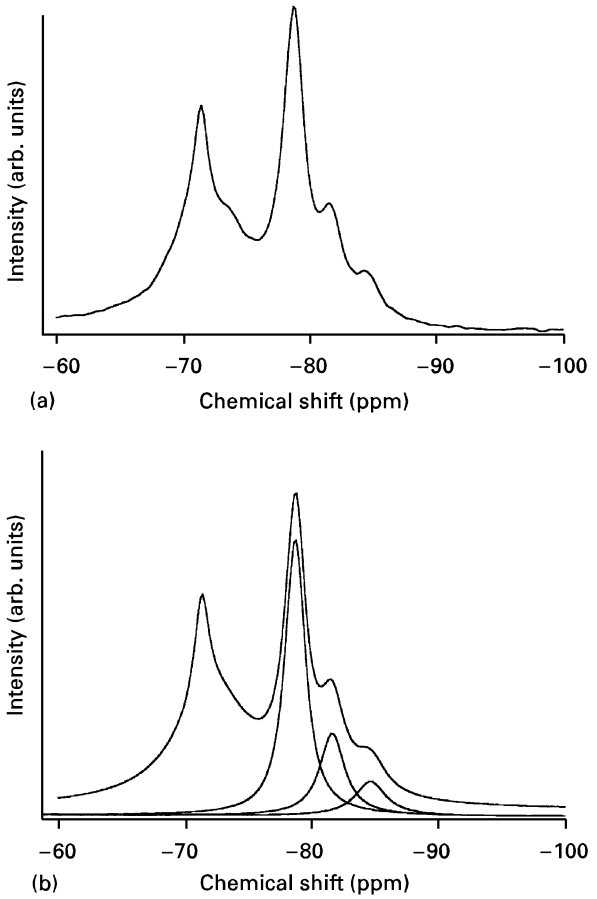

Figure 8 (a) Single pulse ^{29}Si MAS NMR spectrum for the 5M KOH-activated 1/1 slag/WPC blend. The hydrate peaks are well-defined. (b) Results of the deconvolution of (a): the fitted spectrum (the sum of the 5 peaks) plus the three constituent hydrate peaks with chemical shifts of − 78.7 ppm (Q_1), − 81.7 ppm (Q_2(1Al)), and − 84.7 ppm (Q_2(0Al)). MCL = 3.60; Al/Si = 0.12.

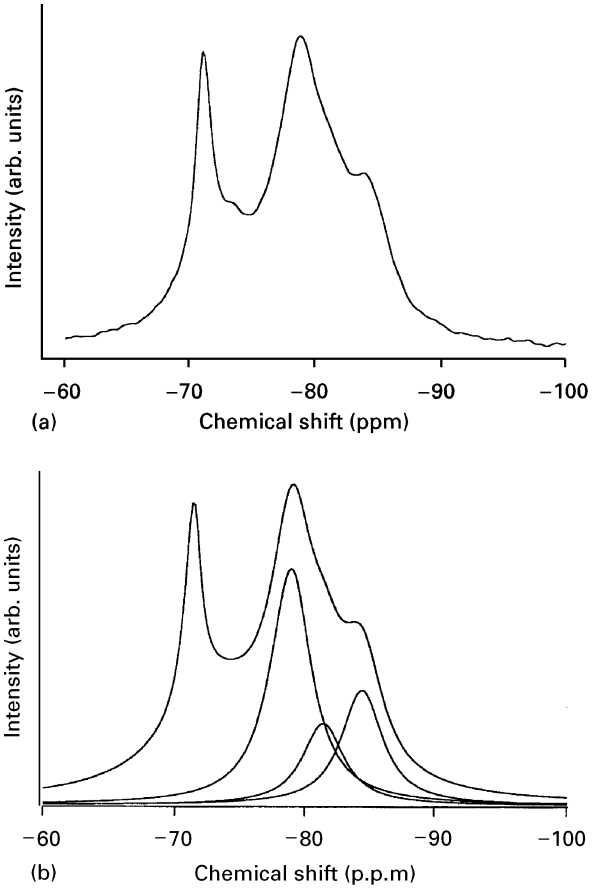

Figure 9 (a) Single pulse ^{29}Si MAS NMR spectrum for the water-activated 1/1 slag/WPC blend. (b) Results of the deconvolution of (a): the fitted spectrum (the sum of the 5 peaks) plus the three constituent hydrate peaks with chemical shifts of − 78.9 ppm (Q_1), − 81.5 ppm (Q_2(1Al)), and − 84.5 ppm (Q_2(0Al)). MCL = 4.05; Al/Si = 0.10.

When the centre bands had been fitted satisfactorily their coefficients were fixed and those for the first order side bands unconstrained, but with the lineshapes and linewidths fixed at the values derived for the main peaks. The intensity values used in calculating the Al/Si ratio and mean chain length thus included components for the centre bands and first order spinning side bands.

The mean chain length (MCL) and Al/Si ratio were calculated from the peak area using Equations 4 and 5:

$$\mathrm{MCL} = \frac{2}{\left(\dfrac{Q_1}{Q_1 + Q_2(0Al) + \frac{3}{2}(1Al)}\right)} \quad (4)$$

$$\mathrm{Al/Si} = \frac{\frac{1}{2}Q_2(1Al)}{Q_1 + Q_2(0Al) + Q_2(1Al)} \quad (5)$$

3.3.1.4 Stage 4. Stages 1 and 2 were repeated for the water-activated pastes. The fitted peaks resulting from the deconvolution of the KOH spectra were then superimposed onto the water-activated spectra. Four peaks were then iteratively fitted to these spectra with their coefficients initially set to those for the KOH peaks. The coefficients for the lineshape and linewidth of the Q_2(1Al) and Q_2(0Al) peaks were set to those for Q_1 i.e., K15 was used instead of K21 and K27, and K16 instead of K22 and K28. Again, when the centre bands had been successfully fitted, the first-order side bands were included.

It is apparent that the KOH- and water-activated spectra are similar except that the hydrate peaks are broader in the case of water activation. The chemical compositions of the C-S-H are quite similar.

Fig. 8(a and b) to 11(a and b) show the results of the deconvolution process; the (a) plots are the raw data and the (b) plots include the fitted spectrum (the sum of the 5 peaks) plus the 3 consituent hydrate peaks. Included in the figure captions are the Al/Si ratio and mean chain length calculated from the results using Equations 4 and 5.

3.3.2 Compositional results and structural implications

Table III summarizes the compositional results. It can be seen that the compositions derived from the deconvolution of the NMR spectra are in excellent agreement with those from TEM. The assumptions made, namely those used in the deconvolution procedure, that there are no chain-terminating Al, and that Al only substitutes for Si at tetrahedral bridging sites, would seem therefore to be well-founded. Al only substituting for Si at tetrahedral bridging sites is certainly true for the water-activated 9/1 blends

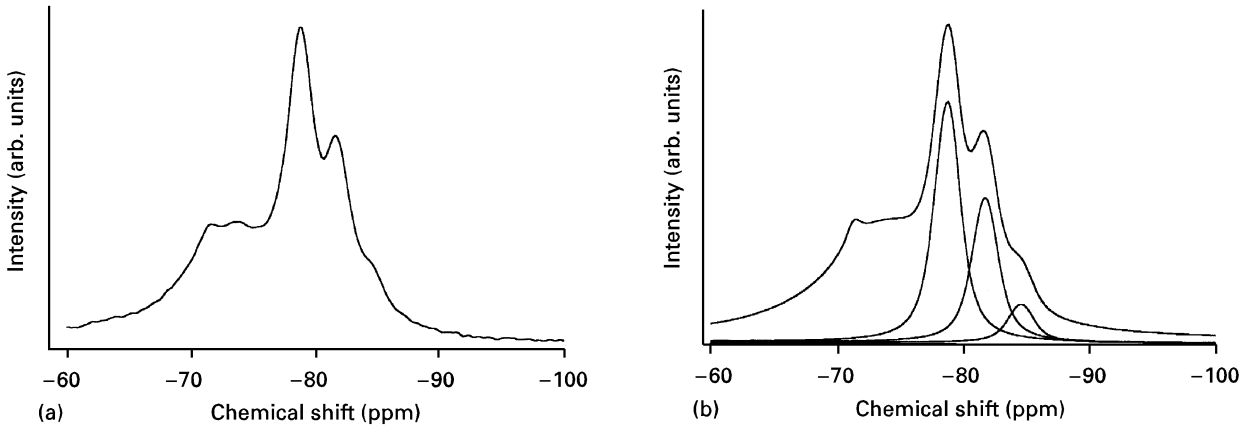

Figure 10 (a) Single pulse ^{29}Si MAS NMR spectrum for the 5M KOH-activated 9/1 slag/WPC blend. The hydrate peaks are well-defined. (b) Results of the deconvolution of (a): the fitted spectrum (the sum of the 5 peaks) plus the three constituent hydrate peaks with chemical shifts of -78.7 ppm (Q_1), -81.7 ppm (Q_2(1Al)), and -84.5 ppm (Q_2(0Al)). MCL = 4.21; Al/Si = 0.17.

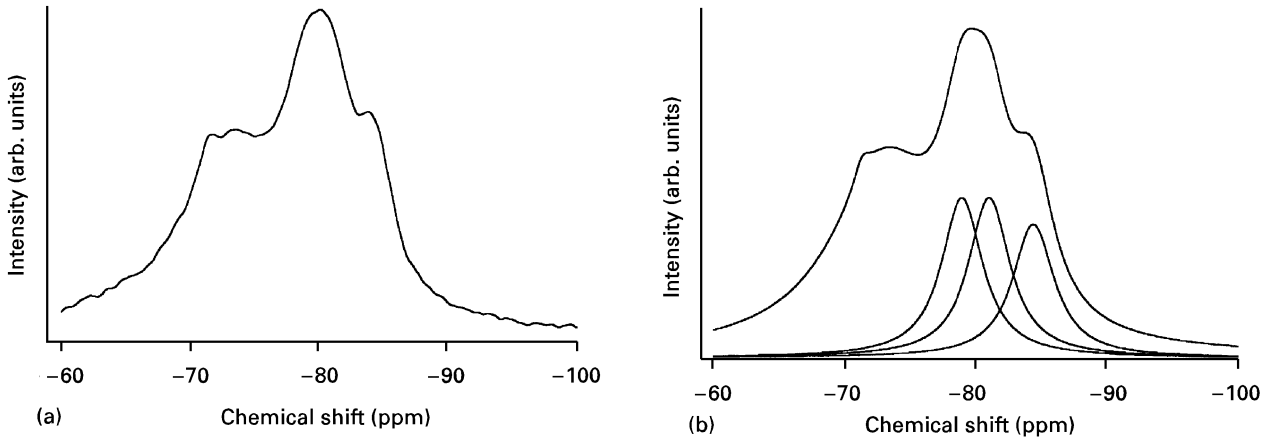

Figure 11 (a) Single pulse ^{29}Si MAS NMR spectrum for the water-activated 9/1 slag/WPC blend. (b) Results of the deconvolution of (a): the fitted spectrum (the sum of the 5 peaks) plus the three constituent hydrate peaks with chemical shifts of -79.0 ppm (Q_1), -81.1 ppm (Q_2(1Al)), and -84.5 ppm (Q_2(0Al)). MCL = 6.45; Al/Si = 0.17.

TABLE III Composition of C-S-H in the blends as determined by TEM and NMR

GGBS:WPC/ activator		TEM Op		TEM Ip		NMR
		Mean	$\pm\,\sigma_{n-1}$ (n)	Mean	$\pm\,\sigma_{n-1}$ (n)	
1:1/water	Ca/Si	1.56	0.17 (27)	1.56	0.12 (21)	
	Al/Si	0.10	0.02	0.11	0.04	0.10
1:1/KOH	Ca/Si	1.63	0.15 (20)	1.47	0.14 (21)	
	Al/Si	0.14	0.04	0.12	0.03	0.12
9:1/water	Ca/Si	1.26	0.05 (20)	1.27	0.09 (20)	
	Al/Si	0.19	0.03	0.15	0.03	0.17
9:1/KOH	Ca/Si	1.14	0.11 (22)	1.16	0.09 (23)	
	Al/Si	0.19	0.05	0.16	0.04	0.17

TEM = composition determined by analytical transmission electron microscopy.
Op = outer product C-S-H.
Ip = inner product C-S-H.
NMR = composition determined by ^{29}Si nuclear magnetic resonance spectroscopy assuming no chain-terminating Al.

because there is no Q_1(1Al) peak on the CP spectrum, Fig. 12a. There is a small peak at ≈ -74 ppm on the CP spectrum for the 1/1 water-activated paste, Fig. 12b. However, this is most porbably due to a hydrated monomeric species, Q_0^H. It is reasonable that Q_0^H might be present in the 1/1 and not 9/1 pastes as it is most likely to be associated with the hydration of the alite phase and not the slag; in a study of a C_3S/SiO_2 hydrated mix using selective ^{29}Si isotropic enrichment the Q_0^H was found to be associated exclusively with the C_3S [30].

Table IV summarizes the NMR results. The Al/Si ratios of the C-S-H in the water- and KOH-activated pastes are very similar but the MCL is slightly greater

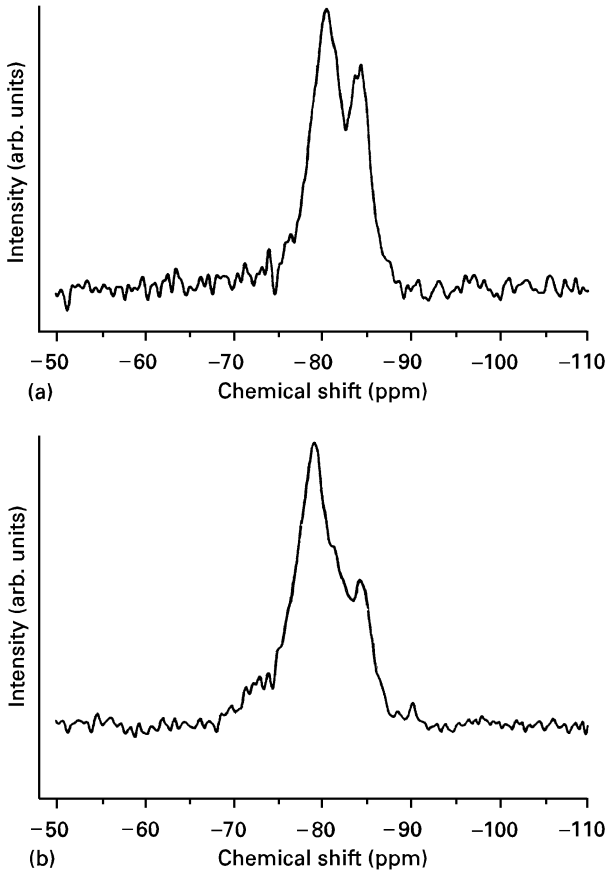

Figure 12 ^{1}H-^{29}Si CP MAS NMR spectra for (a) 9/1 and (b) 1/1 water-activated slag/WPC blends.

TABLE IV Composition and mean chain length of C-S-H gels present in the blends

WPC:BFS	Al/Si	MCL	B(%)	B_{water}/B_{KOH}(%)
1:1/water	0.10	4.05	54	75
1:1/KOH	0.12	3.60	72	
1:9/water	0.17	6.45	63	76
1:9/KOH	0.17	4.21	83	

Al/Si = composition determined by solid-state ^{29}Si nuclear magnetic resonance spectroscopy assuming no chain-terminating Al.
MCL = mean chain length determined by solid-state ^{29}Si nuclear magnetic resonance spectroscopy assuming no chain-terminating Al.
B = bridging tetrahedra occupied by Al/bridging tetrahedra occupied by Al and Si.

in the water system. It is interesting to note that B_w/B_k is the same for the two blends i.e., in both, KOH activation produces four thirds as much Al substitution as does water.

The nature of the NMR spectra and the excellent agreement between the Al/Si ratio measured directly and the Al/Si ratio calculated from the NMR data give considerable confidence in models for the structure of C-S-H based on broken dreierkette chains with Al substituting for Si only at "bridging" sites. The measurements of mean chain length, Al/Si ratio and Ca/Si ratio allow the calculation of some of the parameters of the models. In formula 1 the value of $a/(1-a)$ and $3n-1$ are given directly by the Al/Si ratio and mean chain length respectively but the calculation of the value of y requires, in addition to these

TABLE V Values of y and q based on alternative assumptions about charge compensation

WPC:BFS	y	y'	q	q'
1:1/water	2.82	2.60	0.69	0.71
1:1/KOH	2.51	2.26	0.73	0.76
1:9/water	1.63	1.25	0.87	0.94
1:9/KOH	0.77	0.42	1.06	1.17

y = value of y calculated on the assumption of charge compensation by K^+/Na^+
y' = value of y calculated on the assumption of charge compensation by Ca^{2+}
q = value of q calculated on the assumption of charge compensation by K^+/Na^+
q' = value of q calculated on the assumption of charge compensation by Ca^{2+}.

values, both the Ca/Si ratio of the C-S-H and an assumption as to the nature of the charge compensation for the substitution of Si by Al. If this does not involve Ca^{2+} ions, i.e., it occurs by interlayer K^+ and Na^+, y is given by; $y = (2x(1-a)(3n-1)/n) - 4$ where x is the Ca/Si ratio. The assumption of charge compensation entirely by Ca leads to a slightly smaller value of y given by; $y = ((2x(1-a)-a)(3n-1)/n) - 4$. In the formulation proposed by Taylor [9, 10] for his model of a mixture of tobermorite- and jennite-like structural units,

$$Ca_4[(Si_{6-A-\Delta}R_A\square_\Delta O_{18-2\Delta})H_{2p}$$
$$(Ca, K_2, Na_2)_{2-p+A/2}]_q \cdot (OH)_{8(1-q)} \cdot mH_2O \quad (6)$$

the value of q can be similarly calculated. Values of y and q based on alternative assumptions about charge compensation are given in Table V. The values of y and q represent, in opposite senses, the extent to which the structure contains Ca in excess of that in a simple brokenchain tobermorite-like structure. On the Taylor model a value of q between 0.5 and 1 represents a mixture of jennite- and tobermorite-like units, with $q = 1$ corresponding to pure tobermorite. On the model of Richardson and Groves the incorporation of extra Ca is interpreted in a more general way and y increases as Ca is added to the tobermorite-like structure. With $w = n$ a value of $y = 1$ implies a purely tobermorite-like structure; a value of y below 1 implies that extra H is incorporated in the chains above the value $w = n$.

From the values in Table V it can be seen that as the proportion of WPC in the blend with slag increases the C-S-H incorporates an increasing amount of Ca above that expected for a tobermorite-like structure. It should be noted that this extra Ca cannot simply be present as an intimate mixture of crystalline calcium hydroxide. This is known because in the analysis of the C-S-H gel in the electron microscope, the region analysed is routinely checked by electron diffraction for the absence of Bragg reflections from calcium hydroxide or other crystalline phases. When microcrystalline calcium hydroxide mixed on a scale of 10 nm does occur it is readily detected in the electron microscope as in Fig. 2; other examples of this have been reported [31]. It may also be noted that for a given blend composition the more

crystalline C-S-H in pastes activated by KOH are closer to the tobermorite structure, but only to a modest extent.

4. Conclusions

The C-S-H gels present in both water- and alkali-activated hardened pastes of white Portland cement/blast-furnace slag blends have been studied by solid-state ^{29}Si magic angle spinning NMR spectroscopy and analytical TEM. The C-S-H produced with water-activation is nearly amorphous whilst that produced by alkali-activation is semi-crystalline. Nevertheless, the following conclusions apply to both degrees of structural order: (1) aluminium substitutes for silicon at tetrahedral sites; (2) aluminium only substitutes for silicon in the central tetrahedron of pentameric silicate chains; (3) the results strengthen confidence in dreierkette-based models for the structure of C-S-H. Compositional similarities suggest that these conclusions will be true for OPC/slag blends, and possibly also for OPC/pfa blends indicating that the same structural model applies to C-S-H gels in a wide range of hardened cement pastes.

Acknowledgements

Thanks are due to the Science and Engineering Research Council for funding under Grant No. GR/H64972 and to Dr. C. M. Dobson for encouragement and help with the facilities of the Inorganic Chemistry Laboratory, University of Oxford.

References

1. I. G. RICHARDSON and G. W. GROVES, *J. Mater. Sci.* **27** (1992) 6204.
2. L. S. DENT-GLASSER, E. E. LACHOWSKI, K. MOHAN and H. F. W. TAYLOR, *Cem. Concr. Res.* **8** (1978) 733.
3. N. J. CLAYDEN, C. M. DOBSON, G. W. GROVES and S. A. RODGER, in Proceedings 8th International Congress Chemistry of Cement, Rio de Janeiro, 1986, Vol. 3 (Abla Grafica e Editora Ltda, Rio de Janeiro, 1986) p. 51.
4. S. A. RODGER, G. W. GROVES, N. J. CLAYDEN and C. M. DOBSON, *Mat. Res. Soc. Symp. Proc.* **85** (1987) 13.
5. J. HIRLJAC, Z.-Q. WU and J. F. YOUNG, *Cem. Concr. Res.* **13** (1983) 877.
6. L. S. DENT-GLASSER, E. E. LACHOWSKI, M. Y. QURESHI, H. P. CALHOUN, D. J. EMBREE, W. D, JAMIESON and C. R. MASSON, *ibid.* **11** (1981) 775.
7. H. F. W. TAYLOR, *J. Amer. Ceram. Soc.* **69** (1986) 464.
8. I. G. RICHARDSON and G. W. GROVES, *J. Mater. Sci.* **28** (1993) 265.
9. H. F. W. TAYLOR, *Cem. Concr. Res.* **23** (1993) 995.
10. *Idem*, *Adv. Cem. Bas. Mat.* **1** (1993) 38.
11. R. BRYDSON, I. G. RICHARDSON, D. W. MCCOMB and G. W. GROVES, *Solid State Communications* **88** (1993) 183.
12. I. G. ICHARDSON, A. R. BROUGH, R. BRYDSON, G. W. GROVES and C. M. DOBSON, *J. Amer. Ceram. Soc.* **76** (1993) 2285.
13. Unpublished data.
14. I. G. RICHARDSON and G. W. GROVES, *Cem. Concr. Res.* **22** (1992) 1001.
15. *Idem*, *ibid* **23** (1993) 131.
16. S. A. GREENBERG, T. N. CHANG and E. ANDERSON, *J. Phys. Chem.* **64** (1960) 1151.
17. S. A. GREENBERG and T. N. CHANG, *ibid* **69** (1965) 182.
18. K. FUJII and W. KONDO, *J. Amer. Ceram. Soc.* **66** (1983) C-220.
19. D. L. KANTRO, S. BRUNAUER and C. H. WEISE, *J. Phys. Chem.* **66** (1962) 1804.
20. J. D. BIRCHALL and N. L. THOMAS, *Proc. Brit. Ceram. Soc.* **35** (1984) 305.
21. F. P. GLASSER, E. E. LACHOWSKI and D. E. MACPHEE, *J. Amer. Ceram. Soc.* **70** (1987) 481.
22. I. G. RICHARDSON, A. R. BROUGH, G. W. GROVES and C. M. DOBSON, *Cem. Concr. Res.* **24** (1994) 813.
23. G. ENGELHARDT and D. MICHEL, "High resolution solid state NMR of silicates and zeolites" (Wiley, Chichester, 1987).
24. G. W. GROVES, P. J. LESUEUR and W. SINCLAIR, *J. Amer. Ceram. Soc.* **69** (1986) 353.
25. J. ROCHA and J. KLINOWSKI, *J. Magn. Reson.* **90** (1990) 567.
26. Wavemetrics, IGOR, Lake Oswego, Oregon, 97035, USA, (1992).
27. A. R. BROUGH, D.Phil. thesis, University of Oxford, Oxford (1993).
28. A. M. HARRISSON, N. B. WINTER and H. F. W. TAYLOR, Proceedings 8th International Congress Chemistry of Cement, Rio de Janeiro, 1986, Vol. 4, (Abla Grafica e Editora Ltda, Rio de Janeiro, 1986) p. 170.
29. I. G. RICHARDSON, S. A. RODGER and G. W. GROVES, *Mat. Res. Soc. Symp. Proc.* **176** (1990) 63.
30. A. R. BROUGH, C. M. DOBSON, I. G. RICHARDSON and G. W. GROVES, *J. Mater. Sci.* **30** (1995) 1671.
31. G. W. GROVES and I. G. RICHARDSON, *Cem. Concr. Res.* **24** (1994) 1191.

Received 23 July 1996
and accepted 21 March 1997